J Appl Electrochem (2011) 41:277–287
DOI 10.1007/s10800-010-0235-2

ORIGINAL PAPER

Experimental and computational investigations of corrosion and corrosion inhibition of iron in acid solutions

K. F. Khaled

Received: 4 March 2010 / Accepted: 24 October 2010 / Published online: 5 November 2010

Abstract The corrosion inhibition of iron in 1.0 M HNO_3 by some benzimidazole derivatives, namely 2-(aminomethyl)benzimidazole, 2-(chloromethyl)benzimidazole, and 2-(methylthio)benzimidazole has been studied using weight loss, potentiodynamic polarization, and electrochemical impedance spectroscopy. The results showed that the inhibition efficiency increased with the increase of benzimidazole derivatives concentration and the higher inhibition efficiency is obtained for 2-(aminomethyl)benzimidazole. Quantum chemical calculations and molecular dynamics (MD) simulations were used to evaluate the structural, electronic, and reactivity parameters of the selected benzimidazole derivatives. The MD method has also been used to simulate the adsorption of the selected benzimidazole derivatives and solvent ions on the iron surface.

Keywords Iron · Polarization · EIS · Modeling studies · Acid inhibition

1 Introduction

Acid solutions are widely used in industry, such as acid pickling, industrial acid cleaning, acid descaling, and oil-well cleaning [1]. As the most effective and economic method [2, 3], inhibitors are applied in these processes to control the metal dissolution. Most of the well-known acid inhibitors are organic compounds containing nitrogen, sulfur, and oxygen atoms. The efficiency of these compounds mainly depends on their abilities to be adsorbed on the metal surface with the polar groups acting as the reactive centers. Little attention has been paid to inhibition studies on iron in nitric acid. In nitric acid solutions, the corrosion of iron is much faster than in other mineral acids at comparable concentrations. This is attributed to an autocatalytic process involving some nitrogen oxides, nitrous acid, and/or some iron complexes. At high nitric acid concentrations, passivation of iron takes place. The factors affecting the dissolution and the passivation processes are not fully understood. Use of the organic compounds as corrosion inhibitors in nitric acid, has been scarcely attempted because of the presumption that organic compounds would not be stable in the acid and would show very poor inhibition [4]. The effect of various inhibitors on the corrosion of iron in acid media has been studied. Ammar and Darwish [5] studied the passivation of iron and the effect of some anions, e.g., Br^- and I^- on the passive film. The effect of amides as inhibitors for iron in nitric acid has been reported by Fouda and Gouda [6]. These authors have found that the corrosion process is controlled by the reaction of amides with HNO_3 and not by the surface reaction. The effect of some aminopyrimidine derivatives on the corrosion of 1018 carbon steel in 0.05 M HNO_3 solution has been reported. These inhibitors are adsorbed on the steel surface according to Temkin isotherm [7]. Thiourea derivatives have been used as effective corrosion inhibitors for iron in molar nitric acid [8].

For the inhibition of aqueous metallic corrosion with an organic compound, it is necessary to find a ligand that adsorbs strongly with the metal. To be effective, an

K. F. Khaled (✉)
Electrochemistry Research Laboratory, Chemistry Department, Faculty of Education, Ain Shams University, Roxy, Cairo, Egypt
e-mail: khaledrice2003@yahoo.com

K. F. Khaled
Materials and Corrosion Laboratory, Chemistry Department, Faculty of Science, Taif University, Taif, Hawiya 888, Kingdom of Saudi Arabia

inhibitor must also displace water from the metal's surface, interact with anodic and cathodic reaction sites to retard the oxidation and reduction corrosion reactions, and prevent transportation of water and corrosion-active species to the surface. Molecular modeling has the potential to study this adsorption and possibly identify structurally similar compounds worthy of synthesis and subsequent corrosion testing. Thus, if a molecular mechanics model of the interactions that control the adsorption of a minimized structure with a particular metal can be set up, a measure of the binding (docking or adsorption) energy of the molecule with the metal can be calculated. While this binding energy has no absolute meaning, calculating the relative binding energy of a series of structurally similar ligands may lead to the prediction of other related compounds with potentially more effective inhibiting action.

Results from those studies indicated that molecular dynamics (MD) simulations can provide insights into the design of inhibitor systems with superior properties, and the interaction energy between organic molecule and metal surface given by MD simulations can interpret the difference of inhibition efficiency between organic inhibitors.

In previous studies [9], the compounds containing benzimidazole ring have been shown to be competent corrosion inhibitors in acid medium and this account for their applicability in the petroleum industry, mostly in boiler cleaning and heat exchangers [1, 10].

In continuation of the work on the development of corrosion inhibitors for acidic solutions [11–16], the author has studied the corrosion inhibiting behavior of some benzimidazole derivatives, namely 2-(aminomethyl)benzimidazole (AB), 2-(chloromethyl)benzimidazole (CB), and 2-(methylthio)benzimidazole (MB) as possible corrosion inhibitors against the corrosion of iron (99.9999%) in solutions of nitric acid. The aim of this work is devoted to study the inhibition characteristics of these compounds for acid corrosion of iron 99.9999 by chemical (weight loss), dc polarization, and ac impedance measurements and the impact of their structural and electronic properties on corrosion inhibition by density function theory, DFT. Also, semi-empirical quantum chemical calculations and MD simulations studies were performed to simulate the adsorption of benzimidazole derivatives on the iron surface in an attempt to investigate their corrosion inhibition behavior.

2 Experimental details

Experiments were performed on iron electrode with 99.999% purity (Johnson Matthey Chemicals). The iron rod was welded to iron wire for electrical connection and mounted in Teflon with an active flat disc shaped surface of (0.28 cm^2) geometric area to contact the test solution. Prior to each experiment the iron electrode was abraded using different grit sizes emery papers up to 4/0 grit size to remove the corrosion products, if any, formed on the surface. The iron electrode was cleaned in 18 MΩ water in an ultrasonic bath for 5 min and subsequently rinsed in acetone and bi-distilled water and immediately immersed in the test solution. The benzimidazole derivatives used in this study are as follows:

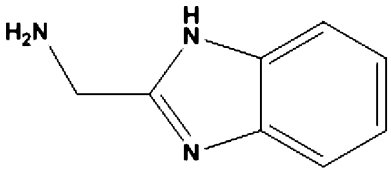

2-(Aminomethyl)benzimidazole (AB)

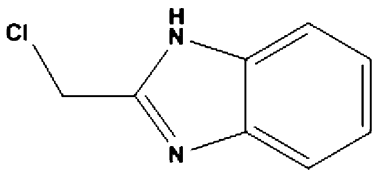

2-(Chloromethyl)benzimidazole (CB)

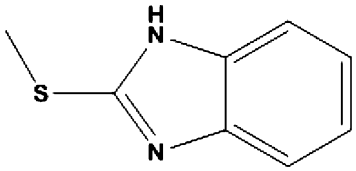

2-(Methylthio)benzimidazole (MB)

All of these compounds were obtained from Aldrich Chemical Co. They were added to 1.0 M HNO_3 (Fisher Scientific) without pre-treatment at concentrations of 3×10^{-5}, 5×10^{-5}, 9×10^{-5}, and 2×10^{-4} M. The working electrode was immersed in these solutions for 1 h before starting electrochemical measurements; this was the time necessary to reach a quasi-stationary value for the open circuit potential.

Weight loss measurements carried out using iron coupons of the same composition, each of dimensions ($2 \times 2 \times 0.1$ cm). Prior to all measurements, the coupons were etched in a 7.0 M HNO_3 solution for 15 s, then washed thoroughly with bi-distilled water, degreased with acetone, washed again with bi-distilled water, and finally dried at room temperature.

The coupons were weighed and suspended in 100 mL of stagnant aerated solutions of 1.0 M HNO_3 solution

containing the studied benzimidazole derivatives at the desired concentrations range (0.03–0.2 mM) at 25 ± 1 °C. At the end of the tests, the coupons were taken out, washed with bi-distilled water, degreased with acetone, washed again with bi-distilled water, dried, and then weighed using an analytical balance (precision: ±0.1 mg). Three measurements were performed in each case and the mean value of the weight loss has been reported. The standard deviation of the observed weight loss was ±1%. The corrosion rate which is the weight loss per unit area, A per unit time, h (w, mg cm^{-2} h^{-1}) is calculated as well as the inhibition efficiency ($\Pi(\%)$) over the exposure time period were calculated according to the following equation:

$$\Pi(\%) = \left(1 - \frac{w}{w_o}\right) \times 100 \quad (1)$$

where w_o and w are the weight loss without and with benzimidazole derivatives, respectively.

Electrochemical measurements were carried out in a conventional electrochemical cell containing three compartments for working, platinum foil (1.0 cm^2), counter and reference electrodes. A Luggin–Haber capillary was also included in the design. The tip of the Luggin capillary is made very close to the surface of the working electrode to minimize IR drop. The reference electrode was a saturated calomel electrode (SCE) used directly in contact with the working solution. The experiments were conducted in a 300 cm^3 cell, open to air, at 25 °C ± 1 using a temperature control water bath. All potential values were reported in volt vs. SCE.

The potentiodynamic current–potential curves were obtained by changing the electrode potential automatically from −514 to −17 mV_{SCE} with a scan rate of 0.1 mV s^{-1}. EIS measurements were carried out in frequency range from 100 kHz to 10 mHz with an amplitude of 5 mV peak-to-peak using ac signals at open circuit potential. EIS spectra were analyzed by Zview impedance analysis software (Scribner Associates Inc., Southern Pines, NC).

Measurements were performed using Gamry Instrument Potentiostat/Galvanostat/ZRA. This includes a Gamry framework system based on the ESA400, Gamry applications that include dc105 for dc corrosion measurements, EIS300 for electrochemical impedance spectroscopy measurements along with a computer for collecting data. Echem Analyst 5.58 software was used for plotting, graphing, and fitting data.

3 Computational procedures

The recent progress in DFT has provided a very useful tool for understanding molecular properties and for describing the behavior of atoms in molecules. DFT methods have become very popular in the last decade due to their accuracy that similar to other methods in less time and with a smaller investment from the computational point of view. In agreement with the DFT, the energy of the fundamental state of polyelectronic systems can be expressed through the total electronic density, and in fact the use of the electronic density instead of the wave function for the calculation of the energy constitutes the fundamental base of DFT [17].

Natural bond orbital (NBO) analysis [18] was performed to evaluate the electron-density distributions. The electron density plays an important role in calculating the chemical reactivity parameters. The global reactivities include electronegativity, χ, which is identified in the finite difference approximation as the negative of the chemical potential μ

$$\chi = -\mu = (I + A)/2 \quad (2)$$

the global hardness η, defined as

$$\eta = (I - A)/2 \quad (3)$$

and the global softness σ as its inverse

$$\sigma = 1/\eta \quad (4)$$

During the interaction of the benzimidazole derivatives with the iron surface, electrons flow from the lower electronegativity benzimidazole derivative molecule to the higher electronegativity iron surface until the chemical potential becomes equalized. The fraction of the transferred electron, ΔN, was estimated according to Pearson [19]

$$\Delta N = \frac{\chi_m - \chi_i}{2(\eta_m + \eta_i)} \quad (5)$$

where the indices m and i refer to iron atom and benzimidazole derivative molecule.

The phenomenon of electrochemical corrosion takes place in the liquid phase, so it is relevant to include the effect of solvent in the computations. Self-consistent reaction field (SCRF) theory [20], with Tomasi's polarized continuum model (PCM) was used to perform the calculations in solution. These methods model the solvent as a continuum of uniform dielectric constant ($\varepsilon = 78.5$) and define the cavity where the solute is placed as a uniform series of interlocking atomic spheres.

The MD simulations were performed using the software, Materials Studio [21]. Fe (001) surface was chosen for the simulation study. The MD simulation of the interaction between molecular benzimidazole derivatives and Fe (001) surface was carried out in a simulation box (14.33 × 14.33 × 28.66 Å) with periodic boundary conditions to model a representative part of the interface devoid of any arbitrary boundary effects. The iron substrate with (001) plane was first optimized to minimum energy, then the addition of the

benzimidazole derivatives molecules near to the surface was carried out and the behavior of the benzimidazole molecule on the Fe (001) surface was simulated using the compass force field. The MD simulation was performed under 25° C, NVT ensemble, with a time step of 0.1 fs and simulation time of 50 ps.

The Discover MD module in Materials Studio 4.3 software from Accelrys Inc. [21] allows selecting a thermodynamic ensemble and the associated parameters, defining simulation time, temperature and pressuring and initiating a dynamics calculation. The MD simulations procedures have been described elsewhere [15]. The interaction energy, $E_{Fe\text{-}inhibitor}$, of the Fe surface with benzimidazole derivatives were calculated according to the following equation:

$$E_{Fe-inhibitor} = E_{complex} - (E_{Fe} + E_{inhibitor}) \quad (6)$$

where $E_{complex}$ is the total energy of the iron crystal together with the adsorbed inhibitor molecule, E_{Fe} and $E_{inhibitor}$ are the total energy of the iron crystal and free inhibitor molecular, respectively. The binding energy of the inhibitor molecule is the negative value of the interaction energy [22], namely:

$$E_{binding} = -E_{Fe-inhibitor} \quad (7)$$

4 Results and discussion

4.1 Weight loss measurements

The effect of addition of different benzimidazole derivatives at various concentrations on the iron corrosion in 1.0 M HNO_3 solutions is studied by weight loss measurements at 25 °C ± 1 after 3 h immersion. The values of inhibition efficiencies $\Pi(\%)$, obtained from Eq. 1, and corrosion rates obtained from weight loss measurements for the three benzimidazole derivatives at different concentrations in 1.0 M HNO_3 are listed in Table 1.

Data in Table 1 indicates that, in all cases, corrosion rate depends on the nature and concentration of the benzimidazole derivatives under investigation. It is found that inhibition efficiency increases with increasing inhibitor concentration, while corrosion rate decreases with inhibitor concentration. The inhibition of iron corrosion can be attributed to the adsorption of the inhibitors at the iron/nitric acid solution interface.

Weight loss measurements demonstrate that all studied benzimidazole derivatives exhibit inhibition properties, and the most effective one is the AB derivative.

4.2 Electrochemical measurements

The electrochemical results of MB, CB, and AB are studied by Tafel polarization and electrochemical impedance measurements, EIS. The inhibition efficiency $\Upsilon_p\%$ was determined by Tafel extrapolation by using the following equation:

$$\Upsilon_p\% = \left(1 - \frac{i_{corr}}{i^o_{corr}}\right) \times 100, \quad (8)$$

where i^o_{corr} and i_{corr} are corrosion current densities in the absence and presence of benzimidazole derivatives, respectively.

Further the inhibitor efficiency Φ% is determined by electrochemical impedance spectroscopy technique.

$$\Phi\% = \left(1 - \frac{R_o}{R}\right) \times 100, \quad (9)$$

where R_o and R represents the uninhibited and inhibited polarization resistance (intersection of the low frequency (LF) inductive loop with x axis), respectively.

Figures 1, 2, and 3 show the cathodic and anodic polarization plots of iron immersed in 1.0 M HNO_3 at 25±1 °C in the absence and presence of different concentrations of benzimidazole derivatives. Electrochemical parameters such as corrosion potential (E_{corr}), anodic Tafel slopes (β_a), and corrosion current density (i_{corr}) are listed in Table 2. The percentage of inhibition efficiency ($\Upsilon_p\%$) were calculated using Eq. 8.

From the results in Table 2, it can be observed that the values of corrosion current density (i_{corr}) of iron in the benzimidazole derivatives-containing solutions were lower than those for the inhibitor-free solution. The corrosion current densities at all inhibitor concentrations are decreased in the order of AB > CB > MB. This indicates on the more beneficial effect of AB on corrosion inhibition

Table 1 Corrosion rate in (mg cm^{-2} h^{-1}), inhibition efficiency Π (%) data obtained from weight loss measurements for iron in 1.0 M HNO_3 solutions without and with various concentrations of MB, CB and AB at 25 ± 1 °C

Inhibitor	Concentration (M)	Corrosion rate (mg cm^{-2} h^{-1})	Π (%)
	Blank	6.33	–
MB	3×10^{-5}	3.15	50.2
	5×10^{-5}	2.58	59.3
	9×10^{-5}	1.88	70.3
	2×10^{-4}	1.32	79.2
CB	3×10^{-5}	2.61	58.7
	5×10^{-5}	2.10	66.8
	9×10^{-5}	1.27	79.9
	2×10^{-4}	0.98	84.5
AB	3×10^{-5}	2.22	64.9
	5×10^{-5}	1.75	72.3
	9×10^{-5}	1.19	81.2
	2×10^{-4}	0.60	90.5

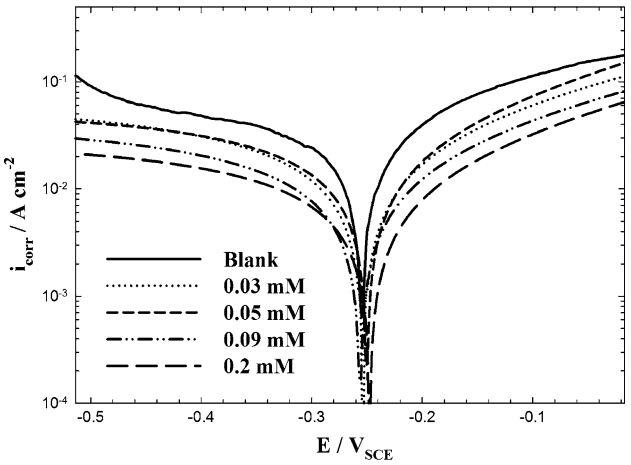

Fig. 1 Potentiodynamic anodic and cathodic polarization curves recorded for iron at a scan rate of 0.1 mV s^{-1} at 25 ± 1 °C in aerated stagnant 1.0 M HNO_3 solutions without and with various concentrations of MB

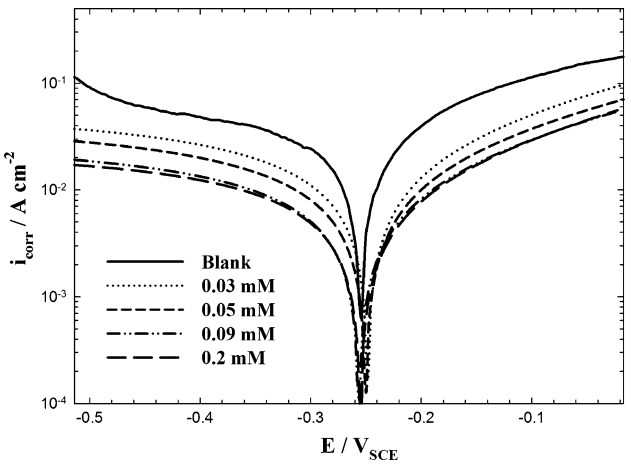

Fig. 2 Potentiodynamic anodic and cathodic polarization curves recorded for iron at a scan rate of 0.1 mV s^{-1} at 25 ± 1 °C in aerated stagnant 1.0 M HNO_3 solutions without and with various concentrations of CB

of iron in 1.0 M HNO_3 solution. As can be seen in Figs. 1, 2, and 3, it was not possible to evaluate the cathodic Tafel slope as there is no visible linear region that prevents linear extrapolation to E_{corr} of the cathodic polarization curves.

It has been shown that in the Tafel extrapolation method, use of both the anodic and cathodic Tafel regions is preferred over the use of only one Tafel region [23]. However, the corrosion rate can also be determined by Tafel extrapolation of either the cathodic or anodic polarization curve alone. If only one polarization curve alone is used, it is generally the cathodic curve which usually produces a longer and better defined Tafel region. Anodic polarization may sometimes produce concentration effects, due to passivation and dissolution, as well as roughening of

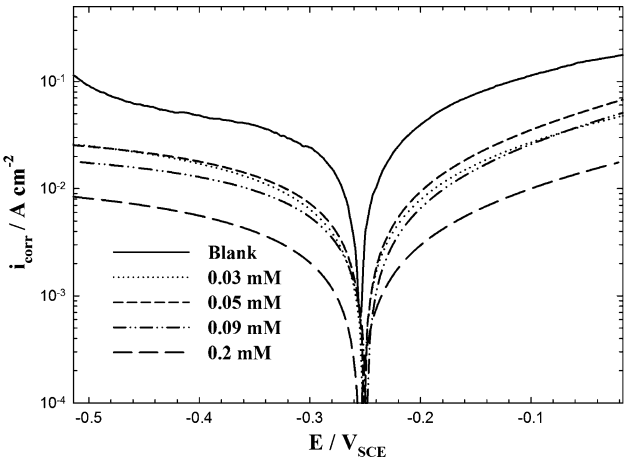

Fig. 3 Potentiodynamic anodic and cathodic polarization curves recorded for iron at a scan rate of 0.1 mV s^{-1} at 25 ± 1 °C in aerated stagnant 1.0 M HNO_3 solutions without and with various concentrations of AB

the surface which can lead to deviations from Tafel behavior.

In the current study; the anodic dissolution of iron in aerated 1.0 M HNO_3 solutions obeys Tafel's law. The anodic curve is, therefore preferred over the cathodic one for the Tafel extrapolation method. However, the cathodic polarization curve displays a limiting diffusion current due to oxygen reduction. Thus, the cathodic process is controlled, by concentration polarization rather than activation polarization, which prevented linear extrapolation of the cathodic curves. The reason why the corrosion current densities were obtained here by extrapolation of the anodic polarization curves to E_{corr}.

In addition, the inflection is quite clear in the cathodic branches, may be due to diffusion control mechanism. Detail description of similar results was discussed in our previous studies [24–26]. It is clear from Figs. 1, 2, and 3 that the corrosion potential E_{corr} shifts with no definite trend indicating that the studied benzimidazole derivatives act as mixed-type inhibitor in HNO_3. Data in Table 2 show that the benzimidazole derivatives act as adsorptive inhibitors, i.e., they reduce anodic dissolution and also, retard the oxygen evolution reaction via blocking the active reaction sites on the iron surface or even can screen part of the electrode and therefore protect it from the action of the corrosion medium [27]. The reaction between iron electrode and nitric acid produces ammonium salts and nitrogen oxides [28–30]. The corrosion of iron in nitric acid is autocatalytic; involving nitrous acid as the intermediate product, and the stability of HNO_2 depends on nitric acid concentration. At $[HNO_3] \leq 0.1$ M, HNO_2 may decompose to nitric oxide; which evolves at the electrode surface [31]. At $[HNO_3] \geq 1.0$ M, HNO_2 becomes stable acid participate effectively in the corrosion process. A simple

Table 2 Electrochemical kinetic parameters, inhibition efficiencies $\Upsilon_p\%$, and rates of corrosion (mpy) associated with Tafel polarization measurements recorded for iron in 1.0 M HNO_3 solutions without and with various concentrations of MB, CB and AB at 25 ± 1 °C

Inhibitor	[Inhib] (mM)	βa (V dec^{-1})	E_{corr} (V(SCE))	i_{corr} (mA cm^{-2})	Υ_p(%)	Corrosion rate (mpy)
	Blank	0.525	−0.255	125	–	57.09 e+3
MB	3×10^{-5}	0.557	−0.253	68.1	45.52	31.15 e+3
	5×10^{-5}	0.405	−0.250	54.5	56.40	24.92 e+3
	9×10^{-5}	0.520	−0.256	43.4	65.28	19.85 e+3
	2×10^{-4}	0.448	−0.249	28.6	77.12	13.08 e+3
CB	3×10^{-5}	0.523	−0.251	53.8	56.96	24.6 e+3
	5×10^{-5}	0.514	−0.249	43.0	65.60	19.69 e+3
	9×10^{-5}	0.521	−0.255	27.3	78.16	12.49 e+3
	2×10^{-4}	0.498	−0.255	23.0	81.60	10.52 e+3
AB	3×10^{-5}	0.587	−0.251	48.5	61.20	22.19 e+3
	5×10^{-5}	0.529	−0.251	36.8	70.56	16.82 e+3
	9×10^{-5}	0.512	−0.255	24.8	80.16	11.33 e+3
	2×10^{-4}	0.601	−0.255	14.3	88.56	6.53 e+3

mechanism assumes the primary displacement of H^+ from solutions:

$$H^+ + e^- \rightarrow H \tag{10}$$

Since the reaction between H^+ and HNO_3 is accompanied by a considerable decrease in free energy, the evolution of H_2 does not occur, and the reduction of HNO_3 will take place:

$$H + HNO_3 \rightarrow NO_2 + H_2O \tag{11}$$

Nitric oxide is adsorbed on the electrode surface, where it will react according to equation:

$$NO_2 + e^- \rightarrow NO_2^- \tag{12}$$

and, in concentrated acid, the following reactions will occur:

$$H^+ + NO_2^- \rightarrow HNO_2 \tag{13}$$

$$HNO_2 + HNO_3 \rightarrow 2NO_2 + H_2O \tag{14}$$

The last reaction is the chain propagating step and the chain termination occurs at the iron surface. It is believed that the passivation of iron start immediately after immersion, where it prevents further attack on the iron surface [32].

However, in aerated nitric acid solutions, dissolved oxygen may also be reduced on iron surface and this will enable some corrosion to take place [33–35]. It is a good approximation to ignore the hydrogen evolution reaction and only consider oxygen reduction in the aerated nitric acid solutions at potentials near the corrosion potential [36]. Cathodic reduction of oxygen can be expressed either by a direct $4e^-$ transfer, Eq. 9:

$$O_2 + 4H^+ + 4e^- \rightarrow 2H_2O \tag{15}$$

or by two consecutive $2e^-$ steps involving a reduction to hydrogen peroxide first, Eq. 17, followed by a further reduction, according to equations [36]:

$$O_2 + 2H^+ + 2e^- \rightarrow H_2O_2 \tag{16}$$

$$H_2O_2 + 2H^+ + 2e^- \rightarrow 2H_2O \tag{17}$$

The transfer of oxygen from the bulk solution to the iron/solution interface will strongly affect the rate of oxygen reduction reaction, despite how oxygen reduction takes place, either in $4e^-$ transfer or two consecutive $2e^-$ transfer steps. Iron dissolves in cold and dilute nitric acid to give ferrous nitrate, water, and nitric oxide [37].

$$3Fe(s) + 8HNO_3 \rightarrow Fe(NO_2)_2 + 2NO + 4H_2O \tag{18}$$

In order to investigate the adsorption and inhibition mechanism of the inhibitors as noted above, electrochemical impedance spectroscopy measurement is performed to study the iron/HNO_3 solution interface characteristic in the same solutions as used in the polarization curve experiments. Figures 4, 5, and 6 show the impedance spectra of iron in 1.0 M HNO_3 solution in the absence and presence of different concentrations of benzimidazole derivatives. Inspection of the data reveals that each impedance diagram consists of three time constants, i.e., a large capacitive loop at high frequency (HF), a small capacitive loop at medium frequency (MF), and a small inductive one at LF values. Moreover, the diameter of the first semicircle increases gradually with the increase of the benzimidazole derivatives concentration from 0.03 to 0.2 mM. Furthermore, the greatest inhibitor concentration of AB (2×10^{-4} M) gives rise to much larger semicircle diameter than other three lower concentrations of AB.

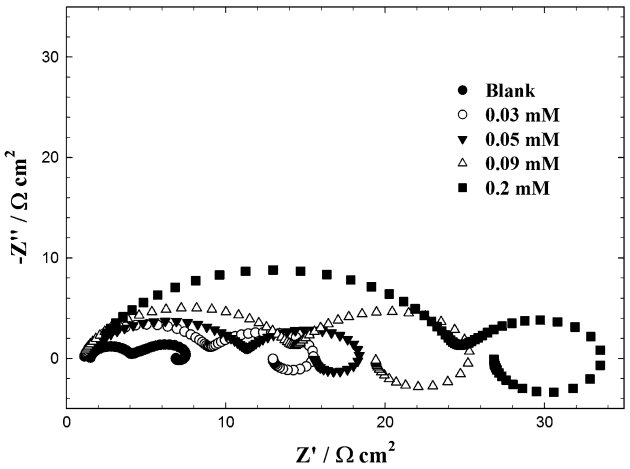

Fig. 4 Nyquist impedance spectra recorded for iron in aerated stagnant 1.0 M HNO_3 solutions without and with various concentrations of various concentrations of MB

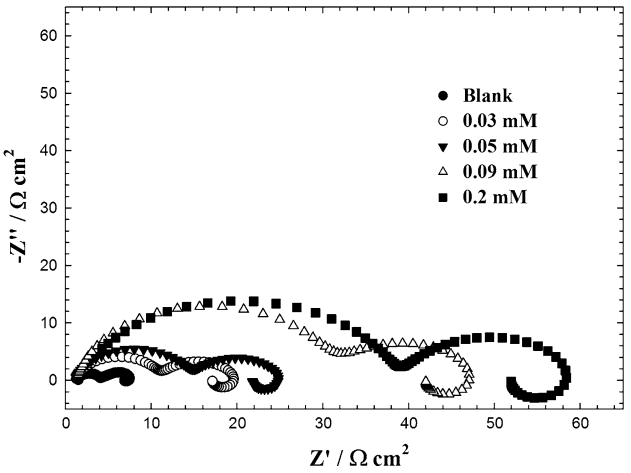

Fig. 5 Nyquist impedance spectra recorded for iron in aerated stagnant 1.0 M HNO_3 solutions without and with various concentrations of various concentrations of CB

The HF capacitive loops in Figs. 4, 5, and 6 are related to the charge transfer process of the metal corrosion and the double layer behavior, and the LF inductive loop may be attributed to the relaxation processes obtained by adsorption of inhibitor on the electrode surface [38]. In other words, the inductive behavior at LF is probably due to the consequence of the layer stabilization byproducts of the corrosion reaction on the electrode surface (for example, $[FeOH]_{ads}$ and $[FeH]_{ads}$) involving inhibitor molecules and their reactive products [39]. It may also, be attributed to the re-dissolution of passivated surface. On the other hand, as is seen, the HF capacitance loops in Figs. 4, 5, and 6 enlarge as the increase of MB, CB, and AB concentrations, respectively. It means that the inhibition efficiency is proportional to the increment of inhibitor concentration.

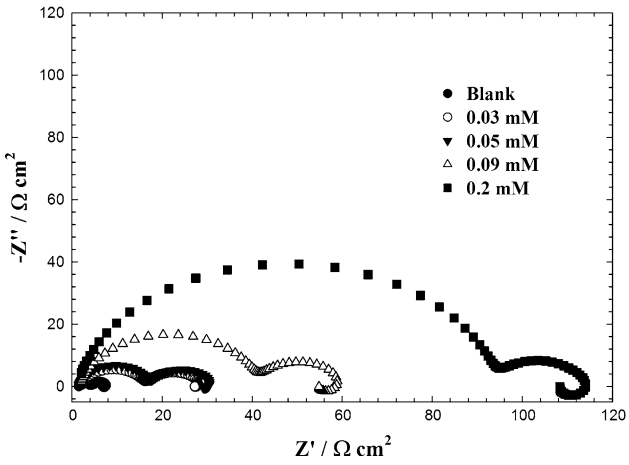

Fig. 6 Nyquist impedance spectra recorded for iron in aerated stagnant 1.0 M HNO_3 solutions without and with various concentrations of various concentrations of AB

Namely, the greater the inhibitor concentration, the higher the inhibition efficiency.

The curves in Figs. 4, 5, and 6 show a similar type of Nyquist plot for iron in the presence of various concentrations of MB, CB, and AB. The Nyquist plots contain a depressed semi-circle, with the center below the real x axis, which sizes are increased by increasing the benzimidazole derivatives concentration, indicating that the corrosion is mainly a charge transfer process [40]. A loop is also seen at low frequencies which could be arising from the adsorbed intermediate products on the iron surface [41]. The depressed semi-circles are the characteristic of solid electrodes and often referred to as frequency dispersion which arises due to the roughness and other inhomogeneities of the surface [42]. It is worth noting that the change in the concentration of benzimidazole derivatives did not alter the style of the impedance curves, suggesting a similar mechanism of inhibition is involved.

Figure 7 shows the equivalent circuit model used to fit the experimental impedance data of iron in 1.0 M HNO_3 containing benzimidazole derivatives, in this case R_s refers to the solution resistance, CPE refers to the constant phase element, R_1 refers to the polarization resistance, and L refers to the inductance. Resistance R_2 and inductivity L may be correlated with a slow LF intermediate process [43]. It should be noticed that the depression of the large semicircles in the complex impedance plane of the Nyquist plots, with the center under the real axis, appears in Figs. 4, 5, and 6. Deviation of this kind, often referred to as frequency dispersion, was attributed to roughness and inhomogeneities of the solid surface. Therefore, a constant phase element (CPE) instead of a capacitive element is used in Fig. 7 to get a more accurate fit of experimental data using generally more complicated equivalent circuits. The impedance, Z, of CPE has the form [44]:

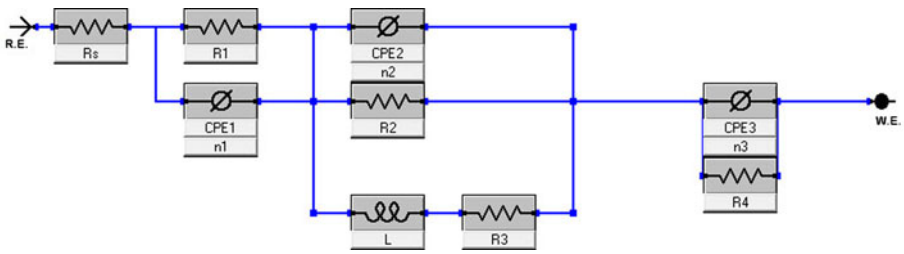

Fig. 7 Equivalent circuit used to fit experimental EIS data recorded for iron electrode in 1.0 M HNO_3 solutions in the absence and presence of various concentrations of the three selected benzimidzole derivatives

$$Z_{\mathrm{CPE}} = [Q(j\omega)]^{-n} \tag{19}$$

where Q is the CPE constant, which is a combination of properties related to the surface and electro-active species, $j^2 = -1$ is the imaginary number, ω is the angular frequency, and n is a CPE exponent which can be used as a measure of the heterogeneity or roughness of the surface. Depending on the value of n, CPE can represent resistance ($n = 0$, $Q = 1/R$), capacitance ($n = 1$, $Q = C$), inductance ($n = -1$, $Q = 1/L$), or Warburg impedance ($n = 0.5$, $Q = W$) [38].

Table 3 contains all the impedance parameters obtained from the simulation of experimental impedance data, including R_s, R_1, R_2, R_3, R_4, L, and CPEs (for the fitting of Q, $n = 0.77$–0.95).

It can be seen from Table 3 that, with the increase of benzimidazole derivatives concentrations (MB, CB, and AB), the inhibition efficiencies increase noticeably, especially the situation of increasing concentration of AB. At the same concentration of inhibitors, the inhibition efficiency of these inhibitors is in the order: AB > CB > MB.

4.3 Computational study

It was shown from chemical and electrochemical studies that the substitution of the hydrogen atom of benzimidazole ring by aminomethyl (–CH_2–NH_2), chloromethyl (–CH_2–Cl), and methylthio (–S–CH_3) groups lead to increase of the inhibition efficiency as shown in Figs. 1, 2, 3, 4, 5, and 6 and Tables 1, 2, and 3. Each benzimidazole derivatives used in the present study contains one benzimidazole ring in their structure. The structure of the rest of the molecule can affect adsorption by its influence on the electron density of the functional group. Studying the structural parameters of the studied benzimidazole derivatives using quantum chemical calculations enable us to focus on parameters that directly influence the electronic interaction of the inhibitor molecules with the metal surface. These are mainly energies of the molecular orbital, E_{HOMO}, E_{LUMO}, ΔE ($E_{\mathrm{LUMO}} - E_{\mathrm{HOMO}}$), and dipole moment μ. The values of calculated quantum chemical parameters such as E_{HOMO}, E_{LUMO}, ΔE ($E_{\mathrm{LUMO}} - E_{\mathrm{HOMO}}$), and μ of the three benzimidazole derivatives are listed in Table 4. As E_{HOMO} is often associated with the electron-donating ability of a molecule, high values of E_{HOMO} are likely to indicate a tendency of the molecule to donate electrons to appropriate acceptor molecules with low energy, empty molecular orbital. Increasing values of the E_{HOMO} facilitate adsorption (and therefore inhibition) by influencing the transport process through the adsorbed layer. Therefore, the energy of the E_{LUMO} indicates the ability of the molecule to accept electrons; hence these are the acceptor states. The lower the value of E_{LUMO}, the more probable, the molecule would accept electrons. As for the values of ΔE ($E_{\mathrm{LUMO}} - E_{\mathrm{HOMO}}$); lower values of the energy difference ΔE will cause higher inhibition efficiency because the energy to remove an electron from the last occupied orbital will be low [1, 45]. For the dipole moment (μ), lower values of μ will favor accumulation of the inhibitor on the metal surface.

The number of expected transferred electrons (ΔN) was also calculated as described elsewhere [46] and depending on the quantum chemical method [47, 48]. Using a theoretical electronegativity, χ value of 4.06 eV/mol according to Pearsons electronegativity scale [49] and global hardness, η value of 0 eV/mol for iron atom [47], ΔN, the fraction of electrons transferred from benzimidazole derivatives to the iron surface, was calculated. Values of ΔN showed inhibition effect resulted from electrons donation. According to Lukovits's study [48], if $\Delta N < 3.6$, the inhibition efficiency increased with increasing electron-donating ability at the metal surface. In this study, the three selected benzimidazole derivatives will be expected to inhibit the iron corrosion through donations of electrons to the iron surface that will be the electron acceptor as indicated in Table 4. AB is found to have the highest HOMO energy and ΔN values, and it had the greatest ability of offering electrons, while MB is found to have the lowest inhibition efficiency, for vice versa.

In the current study, benzimidazole derivatives have been simulated as adsorbate on Fe (001) substrate to find the low energy adsorption sites on the iron surface and to investigate the preferential adsorption of the studied benzimidazole derivatives. The outputs and descriptors calculated by the Monte Carlo simulation are presented in Table 5. The parameters presented in Table 5 include total

Table 3 Electrochemical parameters calculated from EIS measurements on iron electrode in 1.0 M HNO_3 solutions without and with various concentrations of MB, CB and AB at 25±1 °C using equivalent circuit presented in Fig. 7

Inhibitor		R_s (Ω cm^2)	R_1 (Ω cm^2)	CPE_1 ($\mu\Omega^{-1}$ cm^{-2} S$^{-n_1}$)	n_1	R_2 (Ω cm^2)	CPE_2 ($m\Omega^{-1}$ cm^{-2} S$^{-n_2}$)	n_2	L (H cm^2)	R_3 (Ω cm^2)	R_4 (Ω cm^2)	CPE_3 ($m\Omega^{-1}$ cm^{-2} S$^{-n_3}$)	n_3	Φ%
	Blank	1.5	2.5	40.1	0.95	3	30.2	0.9	2	0.8	1.1	15	0.8	–
MB	3×10^{-5}	1.1	7.9	35.3	0.78	3.9	22.1	0.88	1.9	1.1	3.1	8.1	0.89	48.6
	5×10^{-5}	1.2	10.2	30.5	0.80	4.2	20.2	0.87	2.3	1.1	3.3	9.2	0.88	57.2
	9×10^{-5}	0.9	13.5	22.1	0.81	7.9	12.2	0.88	4.2	1.3	3.9	10.2	0.89	65.4
	2×10^{-4}	1.5	21.0	5.5	0.83	10.9	8.1	0.89	4.9	2.2	4.5	11.1	0.78	75.2
CB	3×10^{-5}	1.2	9.8	30.2	0.87	4.1	18.2	0.78	5	1.4	5.1	9.3	0.78	60.6
	5×10^{-5}	1.1	13.6	23.7	0.85	5.3	13.1	0.79	7.5	2.3	5.5	9.1	0.79	69.3
	9×10^{-5}	1.3	29.9	18.1	0.89	9.3	8.3	0.77	8.1	3.1	8.5	9.8	0.77	84.1
	2×10^{-4}	1.6	37.3	3.1	0.81	13.2	5.5	0.76	10.1	5.7	9.1	10.2	0.76	87.1
AB	3×10^{-5}	1.9	14.3	29.1	0.83	3.8	15.3	0.81	9.2	4.1	9.1	15.3	0.81	75.0
	5×10^{-5}	1.5	15.8	25.2	0.89	5.9	11.2	0.83	9.3	4.3	9.3	18.2	0.83	77.2
	9×10^{-5}	1.7	39.8	15.2	0.88	11.6	5.1	0.89	9.5	4.8	9.9	22.1	0.88	87.2
	2×10^{-4}	1.1	93.4	1.5	0.89	16.8	1.5	0.88	10.1	4.9	10.1	29.3	0.87	93.8

energy, in kcal mol^{-1}, of the substrate–adsorbate configuration. The total energy is defined as the sum of the energies of the adsorbate components, the rigid adsorption energy and the deformation energy. In this study, the substrate energy (iron surface) is taken as zero. In addition, adsorption energy in kcal mol^{-1}, reports energy released (or required) when the relaxed adsorbate components (benzimidazole derivatives) are adsorbed on the substrate. The adsorption energy is defined as the sum of the rigid adsorption energy and the deformation energy for the adsorbate components. The rigid adsorption energy reports the energy, in kcal mol^{-1}, released (or required) when the unrelaxed adsorbate components (i.e., before the geometry optimization step) are adsorbed on the substrate. The deformation energy reports the energy, in kcal mol^{-1}, released when the adsorbed adsorbate components are relaxed on the substrate surface. Table 5 shows also (dE_{ads}/dNi), which reports the energy, in kcal mol^{-1}, of substrate–adsorbate configurations where one of the adsorbate components has been removed. The binding energy introduced in Table 5 calculated from Eq. 7.

As can be seen from Table 5, AB gives the maximum adsorption energy found during the simulation process. High values of adsorption energy indicate that AB derivative will adsorb more strongly on the iron surface than CB and MB, respectively. The adsorption density (number of adsorbed molecules in unit area) of benzimidazole derivatives on the Fe (001) substrate is calculated and presented in Fig. 8. AB has the highest adsorption density as indicated in Fig. 8 than the other studied benzimidazole derivatives. Therefore, the studied molecules are likely to adsorb on the iron surface to form stable adsorption layers and protect iron from corrosion. The binding energies as well as the adsorption energy were found to increase in the order AB > CB > MB. The adsorption energy of the studied molecules shows that AB accumulate in higher density that CB and MB, respectively, as indicated in Fig. 8.

As we indicated earlier, the establishment of relationship between inhibition efficiency and molecular structures of organic inhibitors, especially the adsorption orientation of the inhibitors on the metal surface, is of high significance [48]. It has been reported that the adsorption is dependent on the following physicochemical properties of the inhibitor molecule, such as steric factors, functional groups, electron density (i.e., charge distribution) at the donor atoms and π orbital character of donating electrons, and on the natures of substrate metals and the type of interaction between organic molecules and the metallic surface as well [47, 50]. In other words, the efficiency of an organic compound as corrosion inhibitor depends not only on the characteristics of the environment in which it acts, the nature of the metal surface and electrochemical

Table 4 Quantum chemical and molecular dynamics parameters derived for benzimidazole derivatives calculated with DFT method in aqueous phase

	HOMO (eV)	LUMO (eV)	ΔE (eV)	μ (debye)	$I = -E_{HOMO}$	$A = -E_{LUMO}$	$\chi = (I + A)/2$	$\eta = (I - A)/2$	$\Delta N = \frac{\chi_{Fe} - \chi_{inh}}{2(\eta_{Fe} + \eta_{inh})}$
MB	−6.57	−0.43	6.14	2.37	6.57	0.43	3.5	3.1	0.09
CB	−5.63	−0.51	5.12	2.24	5.63	0.51	3.07	2.56	0.193
AB	−5.23	−0.62	4.61	4.801	5.23	0.62	2.93	2.31	0.246

Table 5 Outputs and descriptors calculated by the Mont Carlo simulation for adsorption of benzimidazole derivatives on iron (001)

Inhibitor	Total energy (kcal mol^{-1})	Adsorption energy (kcal mol^{-1})	Rigid adsorption energy (kcal mol^{-1})	Deformation energy (kcal mol^{-1})	dE_{ad}/dNi (kcal mol^{-1})	$E_{Fe-inhibitor}$ (kcal/mol)	$E_{binding}$ (kcal/mol)
MB	−165.1	−210.6	−88.18	−122.4	−210.4	−278.7	278.7
CB	−160.9	−202.5	−83.5	−118.99	−118.99	−345.2	345.2
AB	−167.1	−184.3	−65.07	−119.2	−184.3	−478.1	478.1

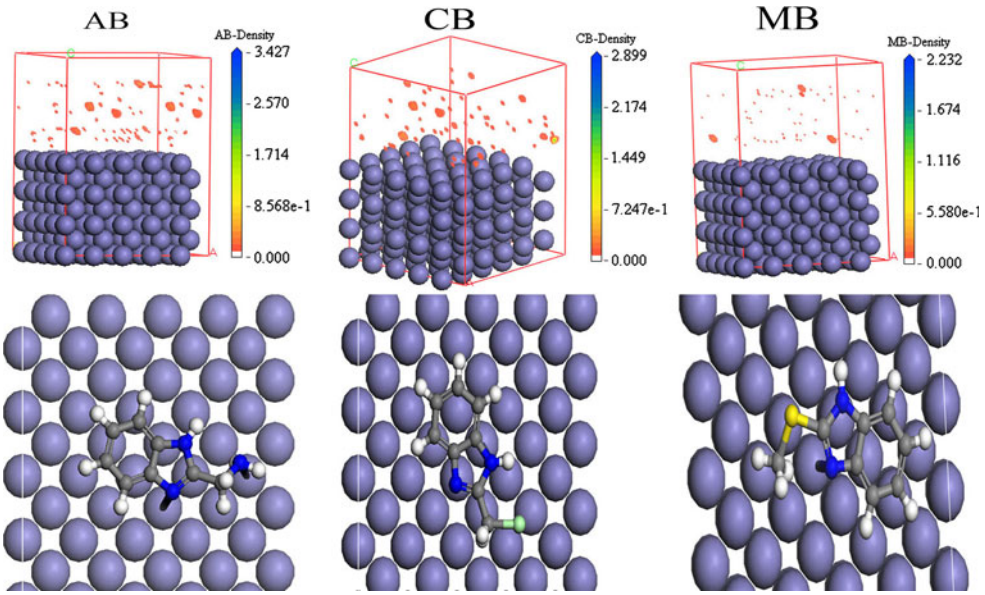

Fig. 8 The adsorption density and the most suitable configuration for adsorption of benzimidazole derivatives on the Fe (001) substrate obtained by adsorption locator module

potential at the interface, but also on the structure of the inhibitor itself, which includes the number of adsorption active centers in the molecule, their charge density, the molecule size, the mode of adsorption, the formation of metallic complexes, and the projected area of the inhibitor on the metallic surface.

Benzimidazole derivatives have proven to be effective inhibitors for the corrosion of iron in acids [11]. The inhibitive effect of these compounds has been attributed to the presence of the hetero-cyclic structure in the benzimidazole moiety as well as in its side chain. For the three inhibitors (MB, CB, and AB) used, there exist the same benzimidazole moiety and different side chains in their molecular structures. The superiority of the structure properties of AB as it has higher E_{HUMO}, lower E_{LUMO}, lower ΔE, and lower μ. Due to the presence of aminomethyl group enhance its adsorption on iron surface more than CB and MB.

5 Conclusions

2-(Aminomethyl)benzimidazole (AB), 2-(chloromethyl) benzimidazole (CB), and 2-(methylthio)benzimidazole (MB) are good inhibitors of corrosion of iron exposed to 1.0 M HNO_3 solution. Their inhibition efficiencies increase in the order of AB > CB > MB. Tafel polarization studies have shown that the selected compounds suppress both anodic and cathodic process and thus act as mixed-type inhibitors. The results of impedance indicate that the value of both polarization resistance and inhibition efficiency tend to increase by increasing

the inhibitor concentration. The inhibitory properties of benzimidazole derivatives were studied by means of density function theory. The calculated electronic parameters involved in the activity of the inhibitors confirmed that the position of the side chain in the benzimidazole moiety affects the pattern of activity. AB shows to be the most effective corrosion inhibitor, the effectiveness of the benzimidazole derivatives following the order: AB > CB > MB.

Acknowledgment Author is grateful for the financial support for the computational work which added to the revised version of this paper provided by the center of research excellence in corrosion at King Fahd University project # CR-03-2010.

References

1. Sastri VS (1998) Corrosion inhibitors: principles and applications. Wiley, Chichester
2. Lagrenée M, Mernari B, Bouanis M, Traisnel M, Bentiss F (2002) Corros Sci 44:573
3. Abdallah M (2002) Corros Sci 45:2705
4. Roebuch AH, Pritchett TR (1966) Mater Prot 7:19
5. Ammar IA, Darwish S (1967) Corros Sci 7:579
6. Fouad AS, Gouda MM (1980) Indian J Chem 19:896
7. Abdallah M, Helal EA, Fouda AS (2006) Corros Sci 48:1639
8. Khaled KF (2010) Appl Surf Sci 256:6753
9. Cruz J, Pandiyan T, García-Ochoa E (2005) J Electroanal Chem 583:8
10. Jones DA (1996) Principles and prevention of corrosion, 2nd edn. Prentice-Hall Inc, New Jersey
11. Khaled KF (2010) Electrochim Acta 55:6523
12. Khaled KF (2010) J Electrochem Soc 157:C116
13. Khaled KF, Fadllalh S, Hammouti B (2009) Mater Chem Phys 117:148
14. Khaled KF, Amin AM, Almobarak NA (2010) J Appl Electrochem 40:601
15. Khaled KF (2009) J Solid State Electrochem 13:1743
16. Khaled KF, Amin AM (2010) Corros Sci 51:1964
17. Andrés J, Beltran J (2000) Química Teórica y Computacional. Universitat Jaume I, Castellón de la Plana
18. Reed AE, Curtiss LA, Weinhold F (1988) Chem Rev 88:899
19. Pearson RG (1988) Inorg Chem 27:734
20. Wong MW, Rrish MJ, Wieberg KB (1991) J Am Chem Soc 113:4776
21. Barriga J, Coto B, Fernandez B (2007) Tribol Int 40:960
22. Mineva T, Parvanov V, Petrov I, Neshev N, Russo N (2001) J Phys Chem A 105:959
23. McCafferty E (2005) Corros Sci 47:3202
24. Khaled KF, Amin AM (2009) Corros Sci 51:1964
25. Amin MA, Khaled KF, Fadl-Allah SA (2010) Corros Sci 52:140
26. Khaled KF (2008) Appl Surf Sci 54:4345
27. Abd El-Maksoud A, Fouda AS (2005) Mater Chem Phys 93:84
28. Abel E (1944) Trans Faraday Soc 40:455
29. Abel E (1936) Monatsh 68:387
30. Evans UR (1960) The corrosion and oxidation of metals. Arnold, London, p 326
31. Divers E, Mellor JW (1952) Comprehensive treatise on inorganic and theoretical chemistry, vol 3. Longman, London, p 90
32. Al-Suhybani AA, Al-Hwaidi IH (1994) Anti-Corros Methods Mater 41:9
33. Quartarone G, Moretti G, Bellomi T, Capobianco G, Zingales A (1998) Corrosion 54:606
34. Bjorndahl WD, Nobe K (1984) Corrosion 40:82
35. Schumacher R, Muller A, Stockel W (1987) J Electroanal Chem 219:311
36. Smyrln WH (1981) In: Bockris JO'M, Conway BE, Yeager E, White RE (eds) Comprehensive treatise of electrochemistry, vol 4. Plenum Press, New York, p 116
37. Jinturkar P, Guan YC, Han KN (1984) Corrosion 54:106
38. Morad MS (2000) Corros Sci 42:1307
39. Kelly EJ (1965) J Electrochem Soc 112:125
40. Bentiss F, Lagrenee M, Traisnel M, Hornez JC (1999) Corros Sci 41:789
41. Solmaz R, Kardaş G, Çulha M, Yazici B, Erbil M (2008) Electrochim Acta 53:5941
42. Bentiss F, Lebrini M, Lagrenée M (2005) Corros Sci 47:2915
43. Gojic M (2001) Corros Sci 43:919
44. Ramelt U, Reinhard G (1990) Electrochim Acta 35:1045
45. Lukovits I, Palfi K, Kalman E (1997) Corrosion 53:915
46. Khaled KF (2003) Electrochim Acta 48:2493
47. Sastri VS, Perumareddi JR (1997) Corros Sci 53:617
48. Lukovits I, Kálmán E, Zucchi F (2001) Corrosion 57:3
49. Pearson RG (1986) Proc Nati Acad Sci 83:8440
50. Soror TY, El-Ziady MA (2002) Mater Chem Phys 77:697